ISSN: 2578-7365

Research Article

Journal of Chemistry: Education Research and Practice

Elaboration and Optimization of Electrodes of Secondary Generators with Active Material of Mixed Oxides of Cobalt and Nickel of Spinel Structure Prepared by the Method of Thermal Decomposition of Nitrates

Mor Cissé, Mamadou Guèye, Modou Gningue Diop and Makhtar Guène*

Department of Chemistry, Cheikh Anta Diop University, Senegal

***Corresponding Author**
Makhtar Guène, Department of Chemistry, Cheikh Anta Diop University, Senegal.

Submitted:2023, May 22;**Accepted**:2023, Jun 19;**Published**:2023, July 14

Citation: Cisse, M., Gueye, M., Diop, M. G., Guene, M. (2023). Elaboration and Optimization of Electrodes of Secondary Generators with Active Material of Mixed Oxides of Cobalt and Nickel of Spinel Structure Prepared by the Method of Thermal Decomposition of Nitrates. *J Chem Edu Res Prac, 7*(2), 506-515.

Abstract

In this study, we prepared particles of mixed oxides of nickel and cobalt of spinel structure of formula NiCo2O4 by the method of thermal decomposition of nitrates. Physical characterizations were made with X-ray diffraction (XRD) and Fourier transform infrared spectroscopy (FTIR). XRD and IRTF analyzes confirmed the nature and crystal structure of the synthesized oxide particles. The study of the optimization of the electrodes in pellets, composed of nickel cobaltite as active material, graphite and Teflon, by the conductivity and the porosity made it possible to show that the electrode of 30% of active material, 5% of teflon and 65% of graphite as the electrode optimized for its use in secondary generators. The electrochemical characterization shows that the optimized electrode has an equilibrium potential of 288.6 V and a capacity of 318 C with an efficiency of 98.9% at a current of 10 mA.

Keywords: Nickel and Cobalt Oxide, Conductivity, Porosity, Secondary Generator Cyclic Voltammetry, Chronopotentiometry

1. Introduction

In the medium and long term, the supply of electrical energy will be confronted on the one hand with a considerable increase in demand, and on the other hand with the reduction in primary resources (oil, gas, etc.). In addition, the production of energy, from its primary resources, is very polluting and has the consequence of global warming, not to mention the many diseases that this causes.

At the same time, the development of portable electronic devices requires accumulators allowing maximum autonomy with a high cycling capacity (charge/discharge).

In such a scenario, current research is increasingly focused on electrical energy conversion and storage systems, the most commonly used of which is the galvanic cell.

The realization of these converters passes, on the one hand, by the research of good electroactive materials for the electrodes and, on the other hand, by the choice of suitable electrolyte. However, in galvanic cells the reactions of reduction and/or release of oxygen intervene in a very notable way in the electrochemical processes [1]. However, the molecule of oxygen is very stable and therefore its reduction requires an energy of very high activation [2]. Similarly, the oxygen release reaction is a limiting factor in the electrolysis of water [3, 4]. Studies carried out by Sing et al, Meadowcroft, Trasati, Chartier, Poillerat et al have shown that the mixed oxides of Ni, Co, Sr, La, etc. have a good electrocatalytic activity in oxygen evolution and/or reduction reactions [5-9]. In addition, they are characterized by their ease of implementation, low cost, good stability and good reactivity [1].

These mixed oxides fall into three families: perovskites, pyrochlores and spinels. Perovskites refer to oxides with the general formula ABO_3 such as calcium titanate ($CaTiO_3$), lead zirconate ($PbZrO_3$) etc... Pyrochlores describe materials of the $A_2B_2O_6$ and $A_2B_2O_7$ type where A and B are generally rare earths or transition metals (Ni, Co, La, Sr…) [10, 11]. As for spinels, they represent oxides with the formula AB_2O_4 and owe this name to the mineral compound $MgAl_2O_4$ (magnesium aluminum oxide or magnesium aluminate). In oxides of spinel structure, O^{2-} anions form a face-centered cubic lattice, defining tetrahedral and octahedral cation sites in this work, we are interested in the mixed oxides of nickel and cobalt of the spinel type of formula $NiCo_2O_4$. The elaboration of the mixed oxide particles was carried out by the method of thermal decomposition of nitrates which consists in dissolving in a container stoichiometric quantities of nitrates to have

a homogeneous mixture and in carrying out a slow evaporation of the solvent by heating in a oven. The structure and morphology of our products have been studied by X-ray diffraction and Fourier transform infrared spectroscopy (FTIR). The optimization of our electrodes was carried out by conductivity and porosity. The electrochemical analyzes were carried out by cyclic voltammetry and chronopotentiometry.

2. Experimental Methods

Thermal decomposition of nitrates: Stoichiometric amounts of cobalt nitrate ($Co(NO_3)_2$, $6H_2O$) and nickel nitrate ($Ni(NO_3)_2$, $6H_2O$) were dissolved in distilled water. This mixture is placed in the oven for 24 hours at a temperature of 90°C for the total evaporation of the crystallization water. The product is then brought to 140°C for calcination. The resulting blackish solid is subjected to a heat pretreatment for 2 hours at 200°C then a final treatment at 350°C for 4 hours to obtain the spinel phase.

Preparation of the electrodes: We used pellet-shaped electrodes. They were prepared with a mixture of active material (mixed oxide of nickel and cobalt), graphite and a small amount of Teflon intended to give them good mechanical strength. The mixture thus obtained was carefully homogenized with a mortar and then introduced into a Beckman-type pellet mold 13 mm in diameter.

Pellets of 200mg were prepared by compacting for 2 minutes, under a pressure of 3 tons per cm2, a homogeneous mixture of 5% by mass of Teflon (10mg), a percentage of mixed oxide of nickel and cobalt varying between 10 and 60% and a percentage of graphite sufficient to complete 100% [12].

3. Results and Discussions

3.1. X-Ray Diffractograms

The crystallinity of our products was examined by X-ray diffraction with a Siemens D-500 type diffractometer configured in Bragg-Brentano mode. The resulting diffractogram shown in Fig. 1 revealed that all the lines index into the spinel-like face-centered cubic system. The 8 peaks corresponding to the reflections of planes 111, 220, 311, 222, 400,422, 511 and 440 and are characteristic diffraction lines of a crystallized phase of spinel type according to the file (JCPDS No. 73-1702). All these peaks (in particular the characteristic one at 311) clearly indicate that the binary mixed oxide crystallized in cubic spinel spatial phases FD3m with a total absence of parasitic peaks like NiO or CoO. This demonstrates the purity of the product.

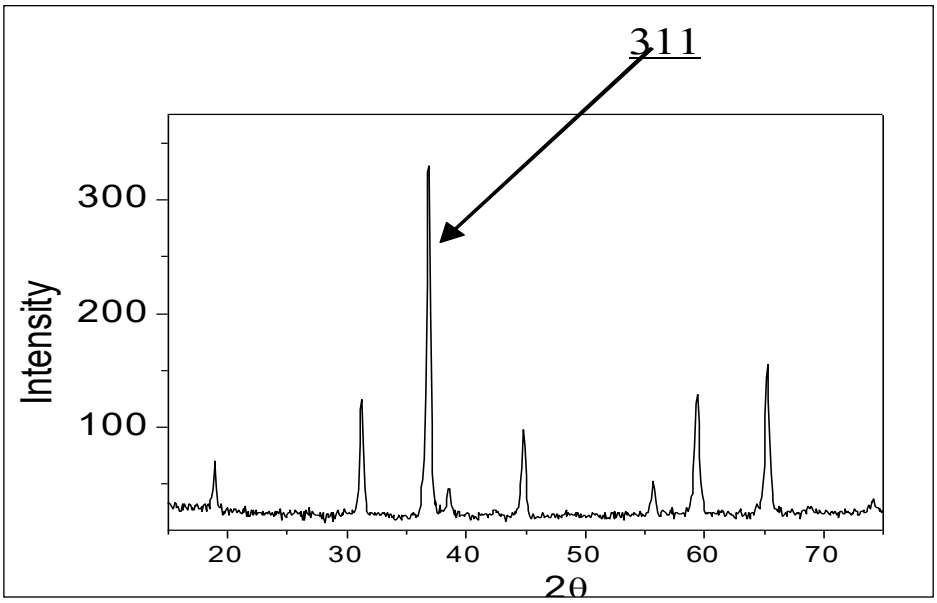

Figure 1: X-Ray Diffractogram

In the following table are recorded the reticular distances and the lattice parameters of $NiCo_2O_4$. The mesh parameters are determined from the reticular distances dhlk of the planes h, l, k by the relation: $a = d_{hlk} (h^2+k^2+l^2)^{1/2}$.

hkl	111	220	311	222	400	422	511	440
d_{hkl}	0,4685	0,2866	0,2443	0,2342	0,2028	0,1654	0,1559	0,1434
a	0,8115	0,8106	0,8102	0,8113	0,8112	0,8103	0,8101	0,8112

Table 1: Values of Reticular Distances and Lattice Parameters

The average value of the lattice parameter obtained, a = 0.8108, shows that the oxide indeed belongs to the face-centered cubic lattice. This value is comparable to that given in the ASTM sheets ($aNiCo_2O_4$ = 0.8128) (JCPDS-ICDD sheets 9-418 and 2-1074).

3.2. Fourier Transform Infrared Spectroscopy (FTIR)

We used FTIR spectroscopy in order to provide additional information about the type of metal oxides as it is known to be a powerful tool in the characterization of mixed oxides [13]. Figure 2 shows the spectrum of $NiCo_2O_4$ oxide prepared by thermal decomposition of nitrates. The two absorption bands strong at 556 cm^{-1} and 657 cm^{-1} correspond to the metal-oxygen stretching of the tetrahedral and octahedral sites respectively, which are characteristic of pure spinel cobaltites [14, 15].

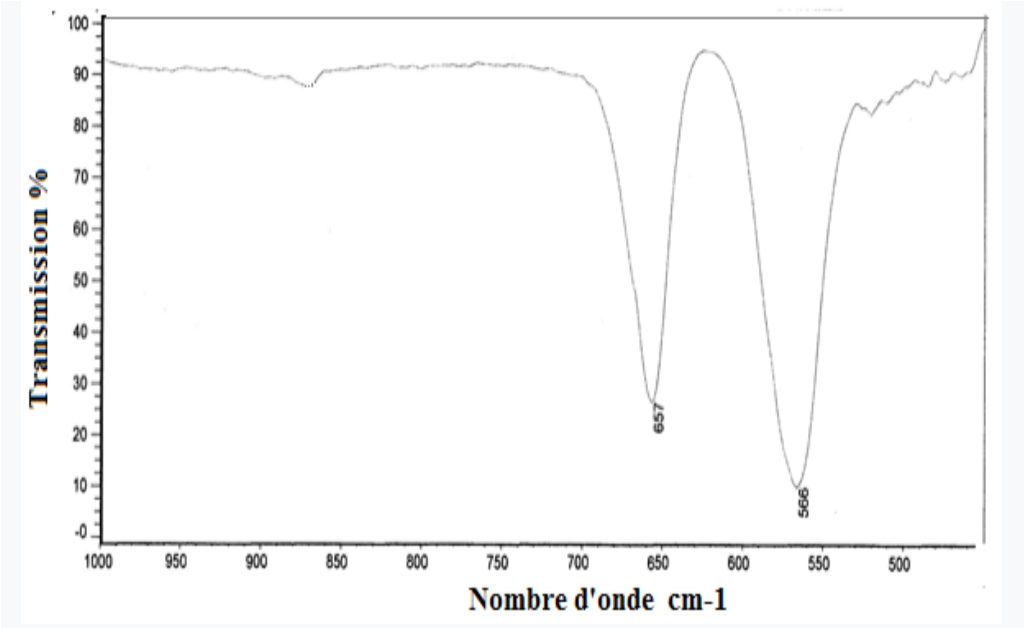

Figure 2: IR Spectrum

3.3. Electrode Electronic Conductivity Measurement

The prepared pellets are introduced into a device called a mercury contact conductivity cell developed by YU et al, see simplified figure (figure 3) [16].

Electronic conductivity measurements were made with a multimeter. The device used makes it possible to directly read the resistance R of the sample; by measuring its thickness e and its section s, we obtain the conductivity by applying the relation : $\lambda e = \frac{e}{Rs}$

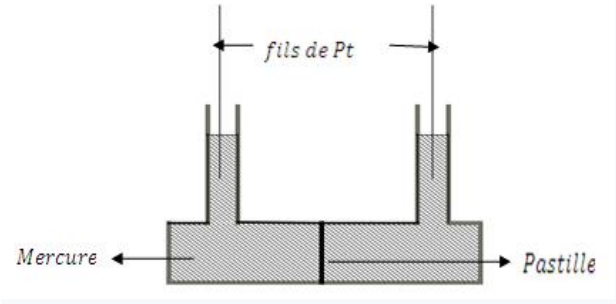

Figure 3: Conductivity Cell

3.3.1. Influence of the Percentage of MA

The results were obtained with pellets whose percentage of MA varies from 10 to 60%. The mass of the pellets is about 200mg.

%Téflon	% MA	S(cm)	e (cm)	R(ohm)	λ
5%(10mg)	10%(20mg)	1,3	0,100	0, 308	0,249
5%(10mg)	20%(40mg)	1,3	0,110	0,467	0, 181
5%(10mg)	30%(60mg)	1,3	0,120	0,700	0,132
5%(10mg)	40%(80mg)	1,3	0,130	0,925	0, 108
5%(10mg)	50%(100mg)	1,3	0,135	1,300	0,079
5%(10mg)	60%(120mg)	1,3	0,120	1,620	0,057

Table 2: Conductivity Values According to % MA

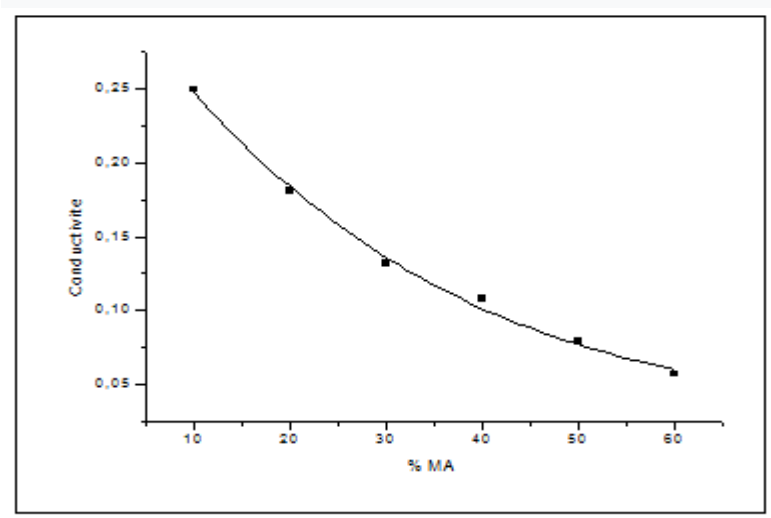

Figure 4: Variation of Conductivity as a Function of % MA

It is noted that the conductivity of the electrode decreases with the increase in the percentage of active material.

3.3.2. Influence of Graphite Percentage

The results were obtained with 200mg pellets whose percentage of graphite varies from 85 to 35%.

%Téflon	% graphite	S(cm)	e (cm)	R(ohm)	λ
5% (10mg)	85%(170mg)	1,3	0,100	0, 308	0,249
5%(10mg)	75%(150mg)	1,3	0,110	0,467	0, 181
5%(10mg)	65%(130mg)	1,3	0,120	0,700	0,132
5%(10mg)	55%(110mg)	1,3	0,130	0,925	0, 108
5%(10mg)	45%(90mg)	1,3	0,135	1,300	0,079
5%(10mg)	35%(70mg)	1,3	0,120	1,620	0,057

Table 3: Conductivity Values According to the % of Graphite

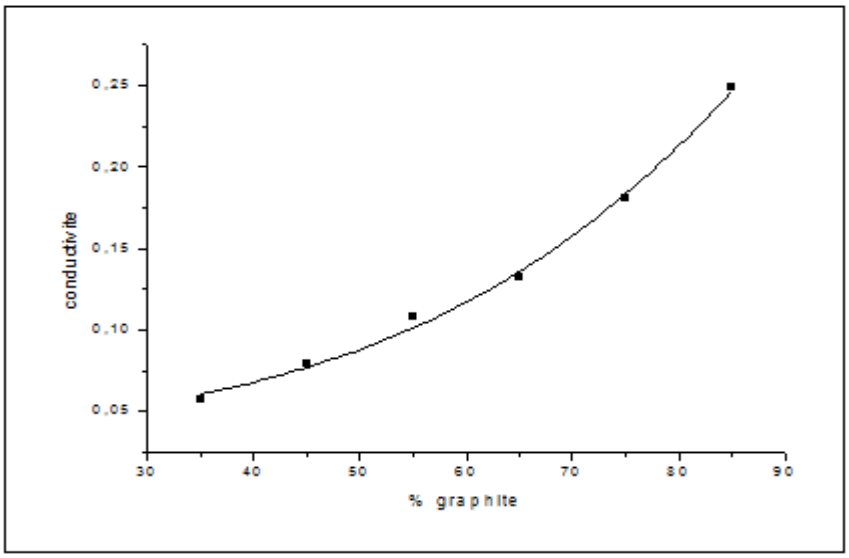

Figure 5: Variation in Conductivity as a Function of % Graphite

The results indicate that the conductivity of the electrode increases with the percentage of graphite.

3.4. Experimental Method for Measuring Porosity

The samples of raw materials, pelleted and prepared as during the measurement of the conductivity are weighed then conditioned in an electrolytic solution of KOH 5M for 48 hours. The samples are then removed and weighed, taking care to quickly wipe off the electrolyte deposited on both sides with filter paper. The mass M of the impregnated sample is thus measured. If Mo was the mass of the dry sample, the porosity is obtained by applying the following relation.

$$\mu = \frac{(M - M_O)1OOO}{M_O}$$

3.4.1. Influence of the Percentage of MA

The following results were obtained with samples in which the percentage of MA varies from 10 to 50%.

% MA	MO (mg)	M (mg)	µ (mg/g d'électrode)
10	199	267	341,7
20	197	253	284,3
30	198	241	217,2
40	196	223	137,7
50	197	219	111,7

Table 4: Porosity Values as a Function of % MA

It appears in Figure 6 that the electrolytic retention capacity (porosity) decreases with the increase in the percentage of MA. This shows a low accessibility of the electrolyte within the electrode due to a low wettability of the active material (cobalt and nickel oxide).

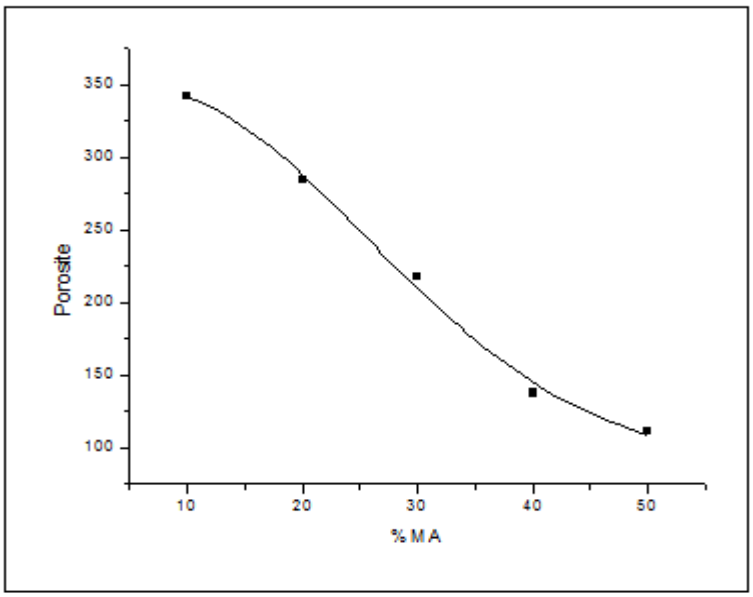

Figure 6: Variation in Porosity as a Function of %MA

3.4.2. Influence of Graphite Percentage

The following results were obtained with samples whose percentage of graphite varies from 85 to 45%, the percentage of Teflon is constant and is equal to 5% (10mg), the percentage of MA varies from 10 to 50% and the mass of each sample is about 200mg.

% graphite	MO (mg)	M (mg)	µ(mg/g d'électrode)
85	199	267	341,7
75	197	253	284,3
65	198	241	217,2
55	196	223	137,7
45	197	219	111,7

Table 5: Porosity Values According to the % of Graphite

Figure 7 shows that the porosity increases with the graphite content in the sample, which means that the graphite provides good electrolytic impregnation, the electrolyte is more accessible within the electrode with the increase in the graphite content.

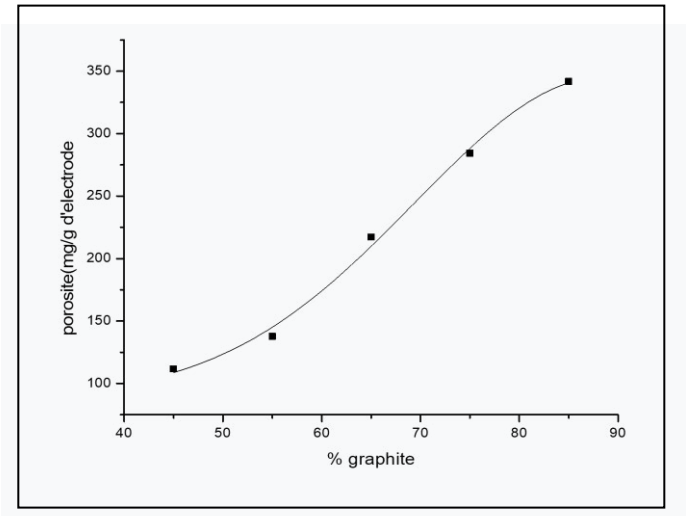

Figure 7: Variation in Porosity as a Function of % Graph

3.5. Electroactivity in a Basic Medium

The electrochemical response (electroactivity) of the optimized electrode was analyzed by cyclic voltammetry in an aqueous medium containing KOH,05M. The study was carried out in a range of potentials between -150 and +600mV/ECS with sweep rates of 10, 20, 30, 40, 50, 60, 70, 80, 90 and 100 mV/s.

The VC curves of the oxide give well defined redox peaks, this indicates that the reaction mechanism in the electrode material is a faradaic process. The anodic and cathodic peaks are between 0.15 - 0.20V and 0.35- 0.45V.

Gong et al. and other researchers have attributed these redox peaks to the reversible reactions of the Co^{4+} / Co^{3+} and Ni^{3+} / Ni^{2+} pairs associated with OH^- ions [17-19]. Since nickel and cobalt ions undergo oxidation and reduction at neighboring potentials, it is difficult to separate the peaks corresponding to these ions in the cyclic voltammetry curve.

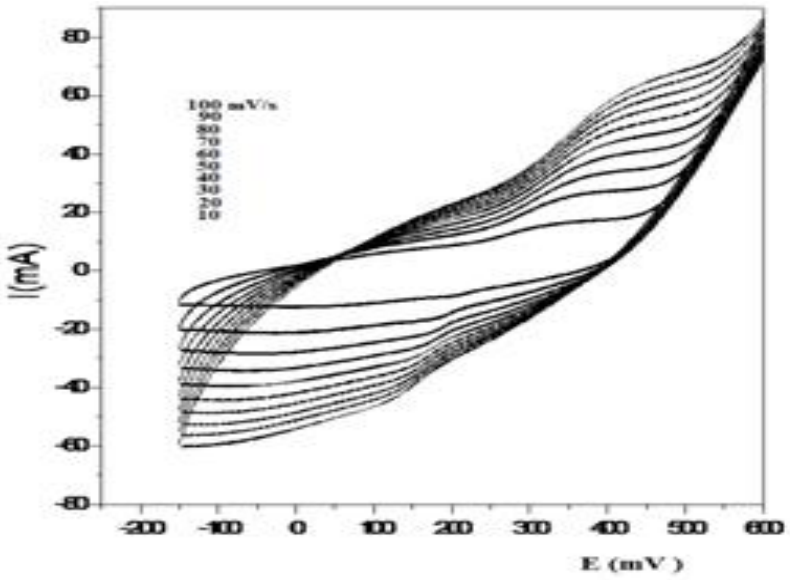

Figure 8: Cyclic Voltammogram of the $NiCo_2O_4$ Electrode from the Speed of 10 mV/s to 100mV/s in Steps of 10 in KOH 5M

3.6. Electrochemical Kinetics and Equilibrium Potential

For the study of the electrochemical kinetics of the electroactive system and its reversibility, we noted the values of the currents (Ip) and potentials (Ep) of the peaks of oxidation and reduction on the voltammograms of figure 8. The results obtained are recorded in Table 6 in order to plot the Ip curves as a function of the square root of the sweep speed ($v^{1/2}$) (Figure 9) [20].

V (mV /s)	$\sqrt{V}$	I_p^{ox} (mA)	I_p^{red}(mA)	E_p^{ox} (mV)	E_p^{red} (mV)	$(E_p^{ox} + E_p^{red})/2$	$(E_p^{ox} - E_p^{red})/V$
100	10	64,56	-43,23	450,84	128,36	289,60	3,22
90	9,48	61,31	-41,19	447,44	131,76	289,60	3,51
80	8,94	57,96	-38,68	444,04	135,16	289,60	3,86
70	8,36	53,88	-36,17	439,14	138,56	288,85	4,29
60	7,74	49,70	-33,29	434,23	141,96	288,09	4,87
50	7,07	45,15	-29,21	427,43	153,66	290,54	5,47
40	6,32	39,77	-26,33	419,12	160,46	289,76	6,47
30	5,47	34,01	-21,32	408,92	168,76	288,84	8,00
20	4,47	26,96	-16,40	397,22	177,07	287,14	11,00
10	3,16	16,65	-08,97	369,02	198,97	283,99	17,00

Table 6

Figure 9 shows that the peaks of the anodic and cathodic currents increase linearly with the square root of the sweep speed which indicates that the redox reactions of $NiCo_2O_4$ are fast in the electrodes and the diffusion of electrolytic ions OH^- is a speed control process [21-24].

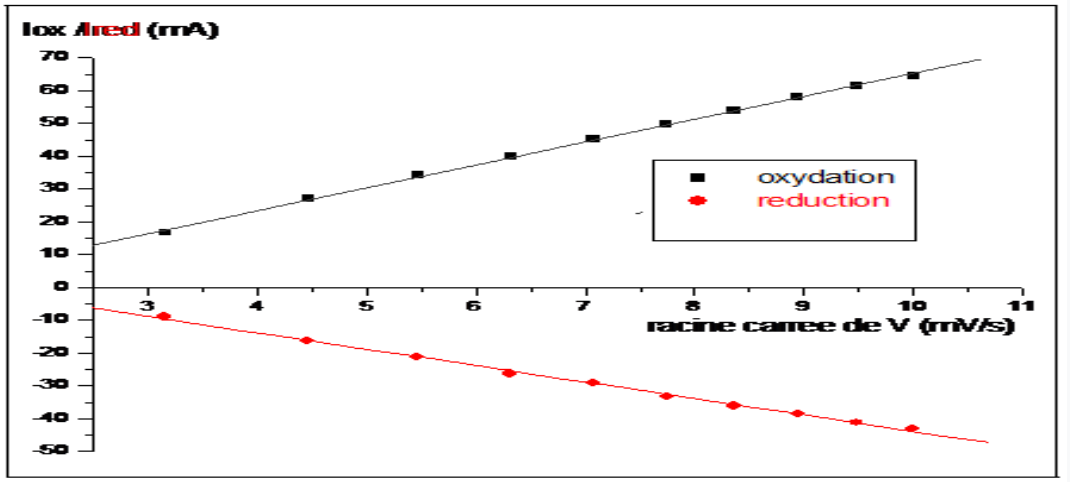

Figure 9: Variation of the Anodic and Cathodic Peak Currents of the $NiCo_2O_4$ Electrode as a Function of the Square Root of the Scanning Speed

The equilibrium potential of the electroactive system studied is obtained by the following relationship [25].

$$Eeq = \frac{Epred + Epox}{2}$$

The values of (Epox + Epred) / 2 (Table 6) remain almost constant and approximate the value of the equilibrium potential Eeq = 288.6 mV of our electrochemical system.

3.7. Determination of Charge by Chronopotentiometry

Constant current chronopotentiometry makes it possible to follow the evolution of the potential of the electrode when it is traversed by an imposed current. The curves obtained are characterized by levels corresponding to the electrochemical transformations of the electroactive compounds within the electrode.

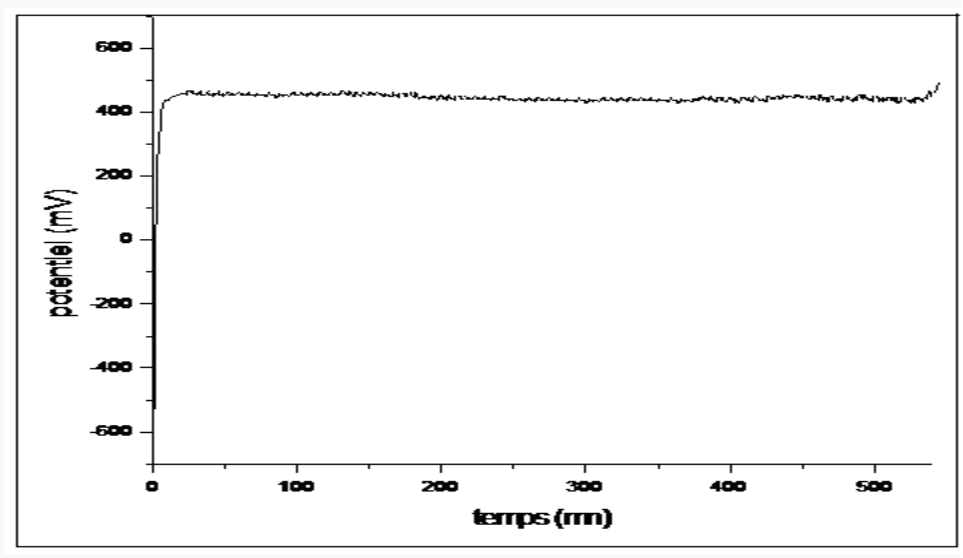

Figure 10: Chronopotentiogram of $NiCo_2O_4$ at 10 mA

By imposing a current of 10mA, we experimentally obtain for the pellet of 30% active material, a capacity Qex = It

Qex = 0.01 × 31800 = 318 C

The average theoretical capacity

$$Q_{th} = \frac{mnF}{M}$$

With m: mass of the active material; M: molar mass of the active ingredient
n: number of electrons exchanged during the electrochemical reaction per mole of active material and F: faraday number (96500)

$$Qth = 0.003 \times 96500 = 321.6C$$

Faradic yield

The faradic efficiency or conversion rate (η) is defined by the ratio of the real capacity to the theoretical capacity

$$\eta = \frac{Q\exp}{Qthéo}$$

$$\eta = \frac{318}{321,6} = 98,9\%$$

4. Conclusion

Nickel cobaltite $NiCo_2O_4$ mixed oxide particles were synthesized by the thermal decomposition method of nitrates. Analysis by X-ray diffraction (XRD) has shown that the nickel cobaltite obtained at 350°C is a pure spinel-type phase whose ideal unit cell is a face-centered cubic lattice with an average value of the parameter of mesh equal to 8.108 Å. Infrared spectroscopy also confirms the nature of the synthesized products. The analysis of the various results on the study of the conductivity and the porosity made it possible to retain that the sample of 30% of active material, 5% of teflon and 65% of graphite as the electrode optimized for its use in secondary generators.

Analysis of the voltammetric curves made it possible to highlight the redox couples involved in the reaction and to determine the equilibrium potential of the electrode Eequ = 288.6 mV. Chronopotentiometry made it possible to determine the experimental capacity of the optimized electrode Qexp = 318 C with a yield of 98.9%. The results obtained attest that the studied composite is a promising electrode for secondary generators.

References

1. Guene, M. (2005). Electrochemical and solid chemistry characterization of mixed oxides of spinel type $Ni_xCo_{3-x}O_4$. Comparative study of physico-chemical properties according to different preparation methods. State thesis, Cheikh Anta Diop University, pp. 118.
2. Sullivan, E. S. M. O., Calvo, E. (1987). Elsevien V27.
3. Hoare, J. P., & Laboda, M. A. (1981). Electrochemical machining. Comprehensive Treatise of Electrochemistry: Electrochemical Processing, 399-520.
4. Damjanovic, A. (1969). Catalysts for the electrochemical generation of oxygen. Pp. 168.
5. Singh, R. N., Koenig, J. F., Poillerat, G., & Chartier, P. (1991). Thin films of CO_3O_4 and $NiCo_2O_4$ prepared by the method of chemical spray pyrolysis for electrocatalysis: Part IV. The electrocatalysis of oxygen reduction. Journal of electroanalytical chemistry and interfacial electrochemistry, 314(1-2), 241-257.
6. Meadowcroft, D. B. (1970). Low-cost oxygen electrode material. Nature, 226(5248), 847-848.
7. Trasatti, S. (1991). Physical electrochemistry of ceramic oxides. Electrochimica acta, 36(2), 225-241.
8. Tiwari, S. K., Samuel, S., Singh, R. N., Poillerat, G., Koenig, J. F., & Chartier, P. (1995). Active thin $NiCo_2O_4$ film prepared on nickel by spray pyrolysis for oxygen evolution. International journal of hydrogen energy, 20(1), 9-15.
9. Ibrahim, K. B., Tsai, M. C., Chala, S. A., Berihun, M. K., Kahsay, A. W., Berhe, T. A., ... & Hwang, B. J. (2019). A review of transition metal-based bifunctional oxygen electrocatalysts. Journal of the Chinese Chemical Society, 66(8), 829-865.
10. Mitchell, R. H. (2002). Perovskites: modern and ancient (Vol. 7, pp. 100-101). Thunder Bay: Almaz Press.
11. Pyrochlores. French Encyclopedia.
12. Gueye, M. (2018). Electrocatalysis of oxygen reduction from composite electrodes based on nanoparticles of mixed oxides of nickel and cobalt $Ni_{0,9}Co_{2,1}$ O_4: physico-chemical and electrochemical characterizations. Thesis of Doctor, Cheikh Anta Diop University, pp. 121.
13. Melendres, C. A., Bowmaker, G. A., Leger, J. M., & Beden, B. (1998). In-situ synchrotron far infrared spectroscopy of surface films on a copper electrode in aqueous solutions. Journal of electroanalytical chemistry, 449(1-2), 215-218.
14. Salavati-Niasari, M., Mir, N., & Davar, F. (2009). Synthesis and characterization of Co_3O_4 nanorods by thermal decomposition of cobalt oxalate. Journal of Physics and Chemistry of Solids, 70(5), 847-852.
15. Alizadeh-Gheshlaghi, E., Shaabani, B., Khodayari, A., Azizian-Kalandaragh, Y., & Rahimi, R. (2012). Investigation of the catalytic activity of nano-sized CuO, Co_3O_4 and $CuCo_2O_4$ powders on thermal decomposition of ammonium perchlorate. Powder technology, 217, 330-339.
16. Yu, L. T., Borreden, M. S., Jozefowiez, M., Delorgey, G., Buvet, R. (1967). Conductivity cell. Journal Polymer Sc. 19.
17. Gong, X., Cheng, J. P., Liu, F., Zhang, L., & Zhang, X. (2014). Nickel–Cobalt hydroxide microspheres electrodepositioned on nickel cobaltite nanowires grown on Ni foam for high-performance pseudocapacitors. Journal of Power Sources, 267, 610-616.
18. Li, Y., & Wu, Y. (2010). Critical role of screw dislocation in

the growth of $Co(OH)_2$ nanowires as intermediates for Co_3O_4 nanowire growth. Chemistry of Materials, 22(19), 5537-5542.
19. Chen, X., Cheng, J. P., Shou, Q. L., Liu, F., & Zhang, X. B. (2012). Effect of calcination temperature on the porous structure of cobalt oxide micro-flowers. CrystEngComm, 14(4), 1271-1276.
20. Diagne, A. Z. (2007). Contribution to the characterization by electrochemical impedance spectroscopy of conductive organic polymers and application of polyaniline to energy storage. Doctoral Thesis University Dakar, pp. 124.
21. Yuan, C., Li, J., Hou, L., Zhang, X., Shen, L., & Lou, X. W. (2012). Ultrathin mesoporous $NiCo_2O_4$ nanosheets supported on Ni foam as advanced electrodes for supercapacitors. Advanced Functional Materials, 22(21), 4592-4597.
22. Singh, A. K., Sarkar, D., Gopal Khan, G., & Mandal, K. (2014). Designing one dimensional Co-Ni/Co_3O_4-NiO core/shell nano-heterostructure electrodes for high-performance pseudocapacitor. Applied Physics Letters, 104(13), 133904.
23. Zhang, X., Xiao, J., Zhang, X., Meng, Y., & Xiao, D. (2016). Three-dimensional Co_3O_4 nanowires@ amorphous $Ni(OH)_2$ ultrathin nanosheets hierarchical structure for electrochemical energy storage. Electrochimica Acta, 191, 758-766.
24. Guéye, M., Mandiamy, P. C. H., Guène, M., & Diagne, A. A. (2017). Nanostructured Ni0. $9Co_2$. $1O_4$ spinel oxide: electrochemical, spectroscopic and morphological investigation. Int. J. Adv. Res, 5(8), 816-823.
25. Diagne, A. A., Fall, M., Guène, M., Dieng, M. M., Deflorian, F., Rossi, S., ... & Della Volpe, C. (2007). Electrochemical impedance spectroscopy of polybithiophene films in an aqueous $LiClO_4$ solution. Comptes Rendus Chimie, 10(6), 558-563.